sensors

MDPI

Article

VOC Detections by p-Type Semiconducting Sensors Using Nano-Sized $SmFeO_3$ Particles

Masami Mori, Ayumu Noguchi and Yoshiteru Itagaki *

Graduate School of Science and Engineering, Ehime University, Matsuyama 790-8577, Japan; mori.masami.mm@ehime-u.ac.jp (M.M.); i843021k@mails.cc.ehime-u.ac.jp (A.N.)
* Correspondence: itagaki.yshiteru.mj@ehime-u.ac.jp; Tel.: +81-89-927-9755

Abstract: Nano-sized $SmFeO_3$ particles are prepared by the pyrolysis of heteronuclear cyano-complex, $Sm[Fe(CN)_6]\cdot 4H_2O$ at a temperature of 600 °C in ozone. The low temperature decomposition followed in ozone successfully yielded fine particles with a high specific surface area of 20.0 m^3/g (sample A). The fine particles were classified into further smaller particles with a unimodal size distribution and this process yielded a high specific surface area of 26.0 m^3/g (sample B). These semiconducting powders were deposited on a sensor electrode by electrophoretic deposition (EPD) and tested on their sensing properties to VOCs. The sensors consisting of samples A and B both showed good responses to ethanol at 285 and 320 °C. The sensor with sample B showed extraordinarily good selectivity of ethanol for toluene at 320 °C. This could be because the detection film of sample B with moderately grown particles selectively reduced the reaction activity of toluene. The sensor with sample B also exhibited good selectivity of ethanol for hexane and dichloromethane.

Keywords: p-type semiconducting sensor; $SmFeO_3$; volatile organic compounds (VOCs); ozone

check for updates

Citation: Mori, M.; Noguchi, A.; Itagaki, Y. VOC Detections by p-Type Semiconducting Sensors Using Nano-Sized $SmFeO_3$ Particles. *Sensors* **2022**, *22*, 5616. https://doi.org/10.3390/s22155616

Academic Editor: Alvise Bagolini

Received: 29 June 2022
Accepted: 25 July 2022
Published: 27 July 2022

Publisher's Note: MDPI stays neutral with regard to jurisdictional claims in published maps and institutional affiliations.

Copyright: © 2022 by the authors. Licensee MDPI, Basel, Switzerland. This article is an open access article distributed under the terms and conditions of the Creative Commons Attribution (CC BY) license (https://creativecommons.org/licenses/by/4.0/).

1. Introduction

Environmental monitoring is an urgent task to control ambient air quality at a variety of locations. Analytical techniques are currently adopted for monitoring systems, but their usage is rather restricted due to their high cost and the large size of the equipment. Use of semiconductor gas sensors instead of analytical has aimed at solving these problems. Since integration of sensor elements is inevitable to add a gas recognition function in ambient air, each element is required to be of small size, low cost, and low energy consumption, as well as high sensing performance. Semiconducting gas sensors convert a reaction of a detected gas with the adsorbed oxygen on the surface into a change in electrical resistance. The semiconducting gas sensors have a simple structure and detect a variety of gasses sensitively [1,2]. So far, n-type semiconducting oxides such as SnO_2 have been widely studied and have already been put into practical use [3]. In the atmosphere, the surface of SnO_2 particles covered with negatively charged adsorbed oxygen forms the depletion layer near the particle surface, inducing a potential barrier for electron transfer at the grain boundaries. The potential barrier is reduced when the target gas reacts to eliminate the adsorbed oxygen. In the case of p-type semiconducting oxides, negatively charged adsorbed oxygen forms a hole accumulation layer near the particle surface, and holes only migrate through the layer. Therefore, it is generally accepted that p-type semiconducting gas sensors tend to be inferior in sensitivity compared to n-type; it is generally accepted that the sensitivity of a p-type semiconductor is the square root of that of n-type [4]. Some p-type semiconductor oxides, however, have a high oxidation catalytic activity [5,6]. Catalytic reactions taking place on a p-type semiconducting oxide effectively change the hole concentration in the accumulation layer. In fact, previous studies have revealed that p-type perovskite oxides such as $LaFeO_3$ [7–10] and $SmFeO_3$ [8–14] were promising materials to detect pollutant gasses such as NO_x with high sensitivity and reliability. A powder of $SmFeO_3$ prepared by the thermal decomposition of the cyano-complex, $Sm[Fe(CN)_6]\cdot 4H_2O$,

has a high surface concentration of Sm^{3+} ions at the A site [9]. The $SmFeO_3$ thick films screen-printed on a comb-type electrode showed a high response, specifically to some target gases [15–17].

A conventional solid-state synthesis requires temperature of over 1000 °C to obtain a single phase of $SmFeO_3$ [12]. As a result, the specific surface area of the $SmFeO_3$ particles decreases owing to grain growth during the high temperature decomposition. The thermal decomposition of the cyano-complex in air allows reduction of pyrolysis temperature to 600 °C, and the specific surface area of $SmFeO_3$ powder prepared by this method is around 10 m^2/g [12]. We previously examined sensor characteristics of $SmFeO_3$ for volatile organic compounds (VOCs) [15]. The $SmFeO_3$ sensor, in that study, exhibited a good response especially to alcohols; $S = R_{VOC}/R_{air}$ was around 30. Since VOC sensing characteristics of p-type semiconductors significantly depend on the oxidation activity for VOC, surface area of the oxide powder will be deeply related to the sensor response. To further increase the surface area of $SmFeO_3$ powder, we, in this study, used ozone-air mixed gas instead of pure air as an oxidizer of the cyano-complex, since ozone has a much larger oxidizing power than air and is assumed to decompose the cyano-complex rapidly at low temperature. In this study, a $SmFeO_3$ powder obtained by the ozone oxidation at 600 °C was found to have a higher surface area than those by conventional air oxidation. We thus examined VOC sensing characteristics of the $SmFeO_3$ powders prepared by ozone pyrolysis.

2. Materials and Methods

The heteronuclear complex, $Sm[Fe(CN)_6]\cdot 4H_2O$, was synthesized at room temperature by mixing aqueous solutions of equimolar amounts of $Sm(NO_3)_3$ and $K_3[Fe(CN)_6]$ under continuous stirring. The resulting precipitate was washed with water, ethanol, and diethyl ether, before drying in air at 50 °C. The complex was set in a tubular furnace and heated at 600 °C for 2 h under ozone gas flow at a rate of 100 mL/min. Ozone gas was generated from compressed air with an ozone gas generator (Funatech SO-250). The products were measured by X-ray diffraction (XRD; X'pert Pro MPD using a Cu Kα radiation, PANalytical) and confirmed the formation of a single phase of the $SmFeO_3$. The obtained $SmFeO_3$ powder was crushed by wet ball milling in ethanol and dried in an oven (sample A). The powder of sample A was then dispersed in acetyl acetone and sonicated for 1 h at room temperature. The suspension was left to stand for 1h to separate it into the components of supernatant and precipitate. The particles in the supernatant layer were collected by a centrifugal separation (sample B). The surface area of the powders was measured by BET analysis using N_2 adsorbent (fine precision surface area and porosimetry system, BELsorp-mini, microtracBEL) and the particle size was analyzed by FE-SEM (S-5500, HITACHI).

Alumina sheets (1.0 mm × 1.0 mm) attached with Pt counter electrodes and micro-heater were used as a sensor substrate. $SmFeO_3$ powder was deposited on the Pt electrode by the EPD method. To prepare an organic suspension of the oxide particle for EPD, 0.04 g of $SmFeO_3$ was dispersed in 10 mL of acetylacetone and 2.5 mg of I_2 was added as a charging agent. The added I_2 reacts with the solvents to form HI and the free protons generated by HI dissociation are adsorbed on the suspended $SmFeO_3$ particle [18]. The mixture was stirred and then sonicated for 30 min at room temperature to obtain a good dispersion. The positively charged $SmFeO_3$ particle is expected to migrate and deposit on the cathodic electrode during the EPD process. The deposition was performed at constant DC voltage of 3 or 5 V for 1–3 min. After the EPD process, the deposits were dried at 70 °C in a drying oven for one day, and then sintered at 600 °C for 3 h with an electric furnace. The surface of the sintered films was observed by FE-SEM.

Figure 1 shows the setup for the sensor tests. The sensor was placed in the stainless chamber and the Pt electrodes and Pt microheater were connected to a d.c. power and a digital electrometer as a heater power source and a resistance meter (Advantest Co., TR8652, Tokyo, Japan). Test gasses were evaporated at a constant temperature from a diffusion tube loaded in a permeator (GASTECH, Co., PD-1B, Ayase, Japan). Compressed air from an oil-free air compressor was introduced in the permeator along with a water bubbler to control

humidity of the test gasses at 50% RH. Test gasses and air were alternately introduced in the chamber with a flow rate of 400 mL/min. The conductance of the elements was measured using a digital electrometer (Advantest, TR8652) at different gas concentrations and operating temperatures.

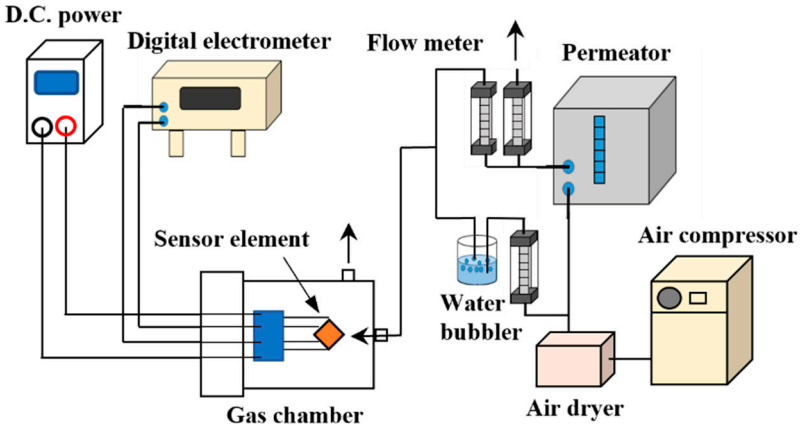

Figure 1. Experimental setup for the sensor test.

3. Results

3.1. Preparation of $SmFeO_3$ Nanoparticles

The XRD pattern of sample A shown in Figure 2 indicates that a single phase of $SmFeO_3$ perovskite was formed by the pyrolysis of the complex at 600 °C in ozone.

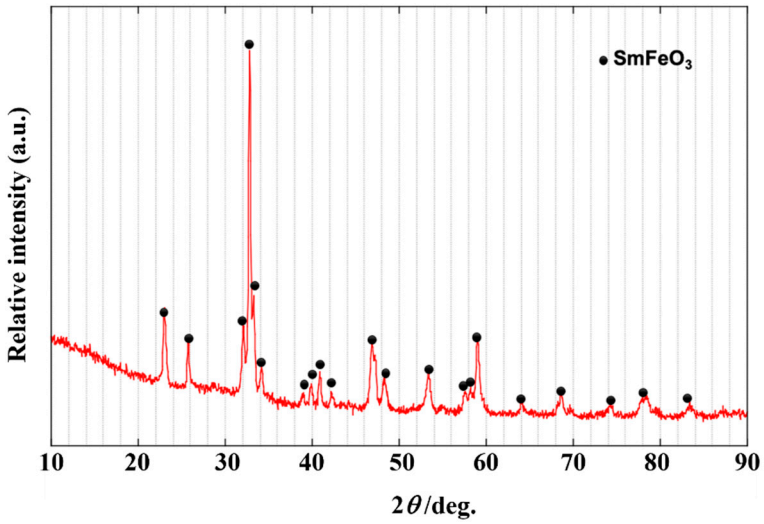

Figure 2. XRD patterns of the $SmFeO_3$ powder (sample A).

Figure 3 shows the volume distributions of the sample powders. Sample A possesses two peaks of distributions centered at 0.40 and 5.5 μm, and the smaller component was predominant. The powder of sample B possesses nearly single modal distribution peaked around 0.17 μm. Median diameters of the powders were evaluated as follows: 0.44 μm (sample A) > 0.17 μm (sample B).

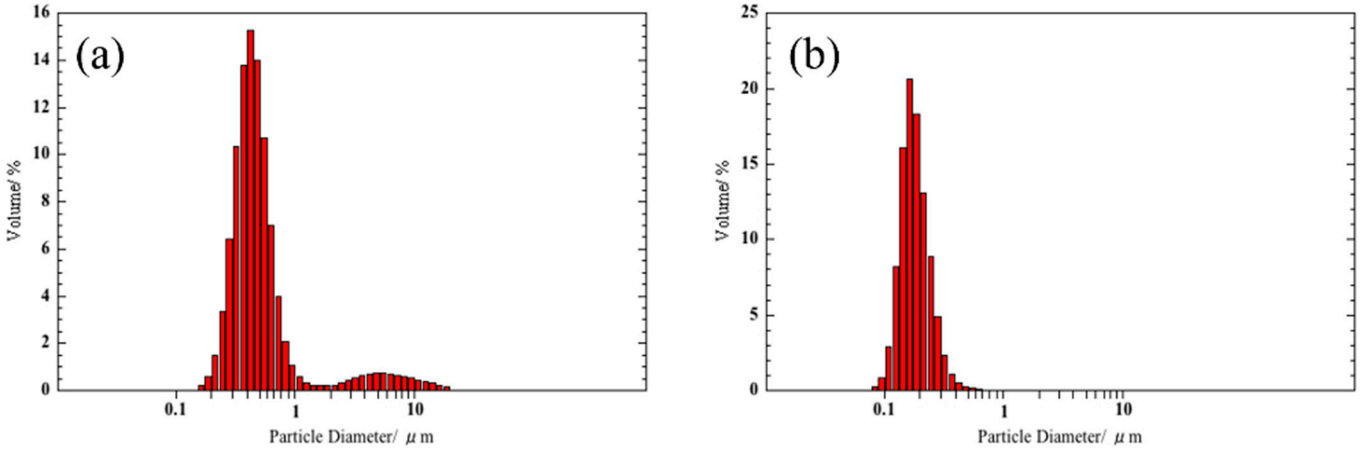

Figure 3. Volume distribution of the classified $SmFeO_3$ powders: (**a**) as balled milled (sample A), and (**b**) the supernatant component of the suspension of sample A (sample B).

Figure 4 shows the nitrogen adsorption isotherms of the powder samples. The adsorption isotherm of sample A shows an intermediate pattern between type II and type IV in which the presence of slight hysteresis can be confirmed, along with macropores (pores of 50 nm or larger) and mesoporous adsorbent (pores of 2 to 50 nm). The hysteresis obtained from sample A is H3 type (IUPAC classification) [19,20], which is a pattern often seen in plate-like aggregates. The powder of sample B can also be judged to be mesoporous adsorbent. The isotherm of this powder shows low pressure hysteresis with no closing point of the hysteresis loop. From the above results, sample A contains a mixture of mesopore particles with different surface areas. The classification operation separated the mixture in sample A into sample B, with a large surface area, and the residue. From the nitrogen adsorption isotherm, specific surface area of samples A and B were evaluated with the BET equation, resulting in 20.0 m^3/g for sample A and 26.0 m^3/g for sample B. It should be noted that specific surface area of the $SmFeO_3$ powder before milling was 17.9 m^2/g.

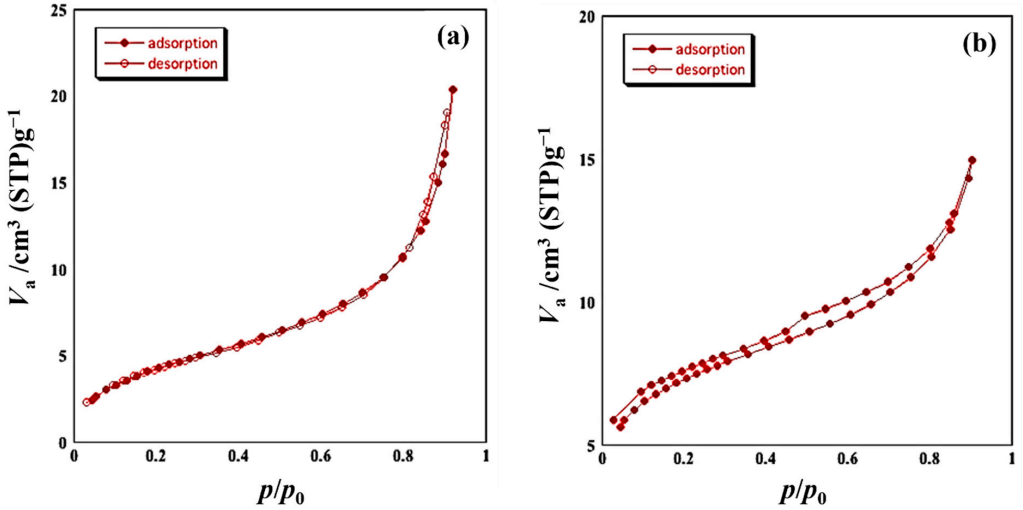

Figure 4. Nitrogen adsorption isotherms of samples A (**a**) and B (**b**) measured at 77K.

Figure 5 shows FE-SEM photographs of samples A and B. $SmFeO_3$ particles with a particle size of 50 nm or smaller were observed for the both samples.

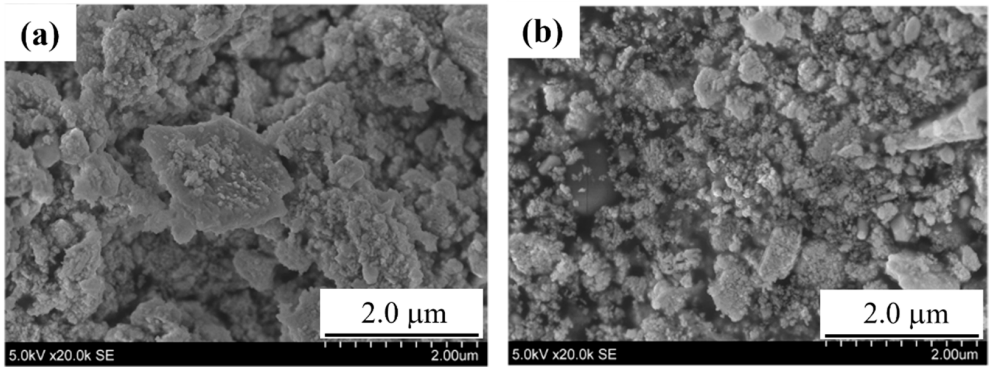

Figure 5. FE-SEM images of the powders of samples A (**a**) and B (**b**).

3.2. Evaluation of Sensor Response Characteristics

In this study the powders of samples A and B were tested as sensor materials. Figure 6 shows SEM photographs of the surface of the sensing layers sintered at 600 °C. The particle size of the powder was smaller in sample B than in sample A, but when the film was formed on the sensor substrate by the EPD method and fired at 600 °C, particle growth due to aggregation occurred. The surface of sample A shows aggregation of particles with a size of 50–60 nm, whereas the particles of sample B clearly coarsened with the neck growth. The detection layers were prepared by the EPD method three time for each sample, resulting in similar morphologies with those in Figure 6.

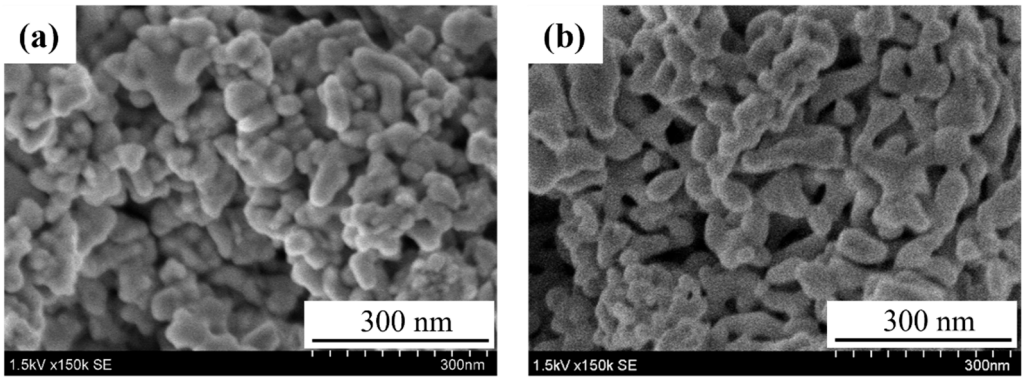

Figure 6. SEM images of the surface of the $SmFeO_3$ detection layers of sample A (**a**) and B (**b**) sintered at 600 °C.

Resistance of $SmFeO_3$ sensors in air is in the range of 1×10^5–1×10^7 Ω at operating temperatures [15]. The present sensors were in the resistance range of 10^7 and 10^6 Ω in air at 285 and 320 °C, respectively. For this reason, we, in this study, set temperature of sensor operation to 285 and 320 °C. Figure 7 shows the transient response curves of the sensors in 5 ppm ethanol at 320 °C. The resistance value of sample A in air was 1×10^7 Ω, and that of sample B in air was 1×10^6 Ω. The difference in the resistance in air may be ascribed to the surface morphology, where sample B showed a more sintered phase. It should be noted that resistance values in dry air are about a half of those in wet air. Li et al. [21] reported on the humidity property of MoS_2@CuO heterogenous photocatalyst. They proposed that the separated holes by photo-illumination are captured by water to form proton and hydroxyl radical Equation (1). This reaction, if taking place on the surface of $SmFeO_3$, would increase resistance of $SmFeO_3$. At present, we are investigating the humidity dependence of the VOC sensing property.

$$h^+ + H_2O \rightarrow H^+ + OH \quad (1)$$

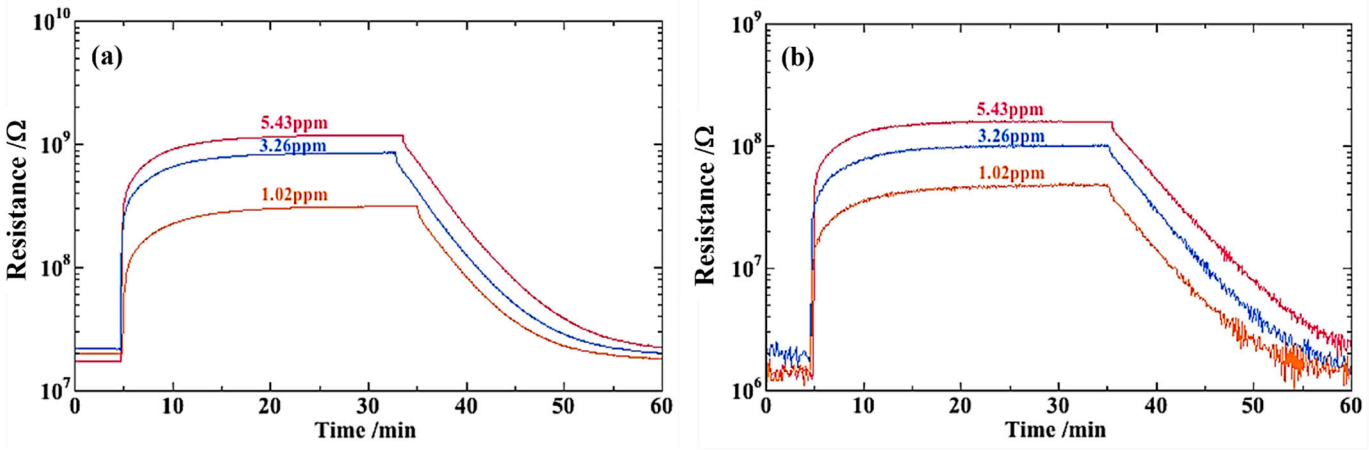

Figure 7. Transient response curves of the sensors with sample A (**a**) and B (**b**) in ethanol at 320 °C.

The 90% response time was 1–2 min, but the recovery time when switching from ethanol to air was very slow, i.e., more than 20 min to return to the resistance in air. Both the sensors exhibited rapid responses from air to ethanol. Recovery from ethanol to air was very slow and recovery time is >20 min. This is due to reaction products, CO_2 and/or H_2O, strongly adsorbed on the surface of the $SmFeO_3$ particles. It should be noted that a signal fluctuation was observed in Figure 7 under the air flow. The cause of this phenomenon is still unknown, but possibly due to an instability of the electrometer induced by an interference from peripheral devices such as a switching timer or others.

Figure 8 shows the responses of the sensors with samples A and B in ethanol and toluene at 285 and 320 °C. The sensor responses are higher at 285 °C than at 320 °C in the sensor with sample A, and vice versa in sample B. The response of sample A to 5 ppm ethanol reached 145, and that in 5 ppm toluene was about 60. On the other hand, the sensor response with sample B is about 125 to 5 ppm ethanol at 320 °C, but the response to 5 ppm toluene is no more than 25 which is much lower than that in the sensor with sample A. It was thus revealed that a $SmFeO_3$ fine particles (samples A and B) can both detect ppm level ethanol with the outstandingly high response. Sample B is more effective to detect ethanol selectively for toluene. The power law is widely accepted in semiconducting sensor where sensor resistance is related to the power of gas concentration [22], hence $R = aP^n$, where a and n are constants, and P is partial pressure of a target gas. The response curves in Figure 8 were thus re-plotted in Figure 9 with a log-log plot to obtain the constants in the power law. The log-log plot showed a good linearity and constants a and n were obtained as summarized in Table 1. Clearly a-values correlate to sensitivity to each VOC as seen in the concentration dependence curves in Figure 8. It seems that the difference in a-values of sample A is smaller than that of sample B. The a-value of the sensor with sample B in ethanol at 320 °C is specifically large, resulting in the high selectivity to ethanol at 320 °C. As regards n-values, those of sample A are close to 1 except for toluene at 320 °C. If VOCs in gas phase behave according to the Henry's law, the amount of adsorption of VOCs is expected to be proportional to partial pressure of the gasses. The sensor with sample A shows responses nearly proportional to concentration of VOCs, suggesting that surface adsorption process of VOC or reaction products are predominant in the sensor mechanism. The fact that the sensor response increases with decreasing temperature is consistent with the above mechanism. On the other hand, the n-values of sample B are significantly smaller than those of sample A, and the sensor response increases with increasing temperature in the case of sample B. This indicates that oxidation reaction of the VOCs is rather dominant in sample B. Although sample B possesses larger specific surface area than sample A, it moderately coarsened during the heating process at 600 °C. This particle growth may reduce catalytic activity to both VOCs, especially to toluene. We previously examined catalytic activity and sensor response of Sm_2O_3 loaded $SmFeO_3$ powders to 30 ppm ethanol

and toluene [23]. The catalytic activity of toluene and the sensor response largely depended on the amount of Sm_2O_3 added.

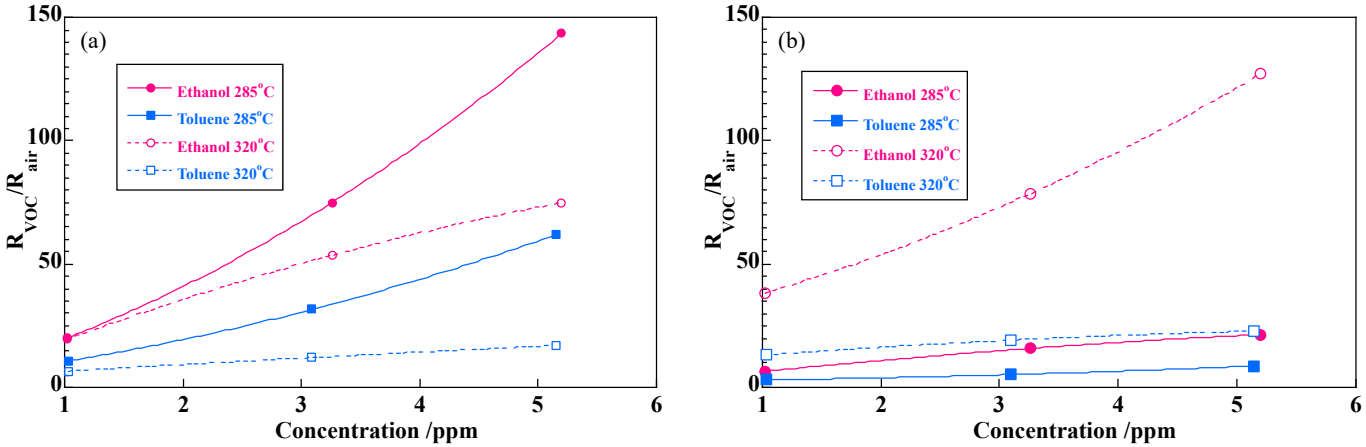

Figure 8. Concentration dependences of sensors responses (R_{VOC}/R_{air}) in ethanol and toluene: (**a**) sample A and (**b**) sample B at 285 and 320 °C.

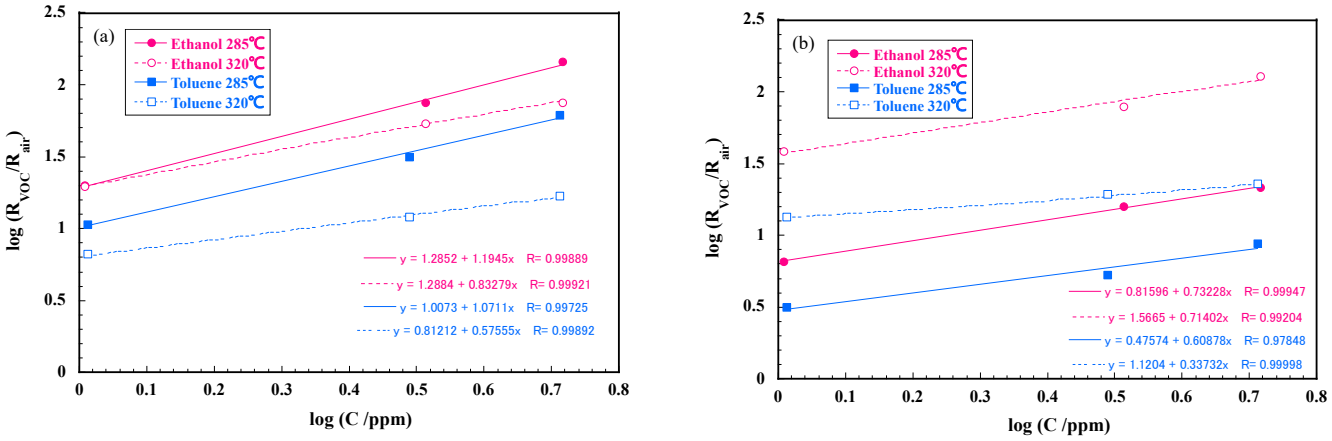

Figure 9. Log-log plots of concentration of ethanol and toluene vs. sensor responses at 285 and 320 °C with sample A (**a**) and sample B (**b**).

Table 1. Characteristic parameters of a and n assuming $R_{VOC}/R_{air} = aP^n$ for the sensors with samples A and B.

Target Gas	Temp. (°C)	Sample A		Sample B	
		a	***n***	***a***	***n***
Ethanol	285	19.3	1.19	6.55	0.732
	320	19.4	0.833	36.9	0.714
Toluene	285	10.2	1.07	2.99	0.609
	320	6.49	0.576	13.2	0.337

This indicates that Sm^{3+} acts as an adsorption site of toluene and catalytic activity and sensor response strongly depends on the amount of toluene. On the other hand, ethanol, having slight acidity, may adsorb more favorably on the Sm^{3+} ion, having slight basicity, regardless of the number of Sm^{3+} ions on the surface. The sensing mechanism of VOC on the different morphology of semiconducting film should be discussed more quantitatively. The present research, however, gave us one qualitative conclusion: that a slightly agglomerated surface effectively suppresses the amount of toluene adsorption, but this is not the case in ethanol, and provides a large difference in sensor response between

ethanol and toluene. Figure 10 shows the sensor responses of the sensor with sample B to 4 types of VOCs: ethanol (alcohol), hexane (aliphatic hydrocarbon), dichloromethanes (organic halide), and toluene (aromatic hydrocarbon). The sensor with sample B also exhibited high selectivity to ethanol among these VOCs, especially at 320 °C.

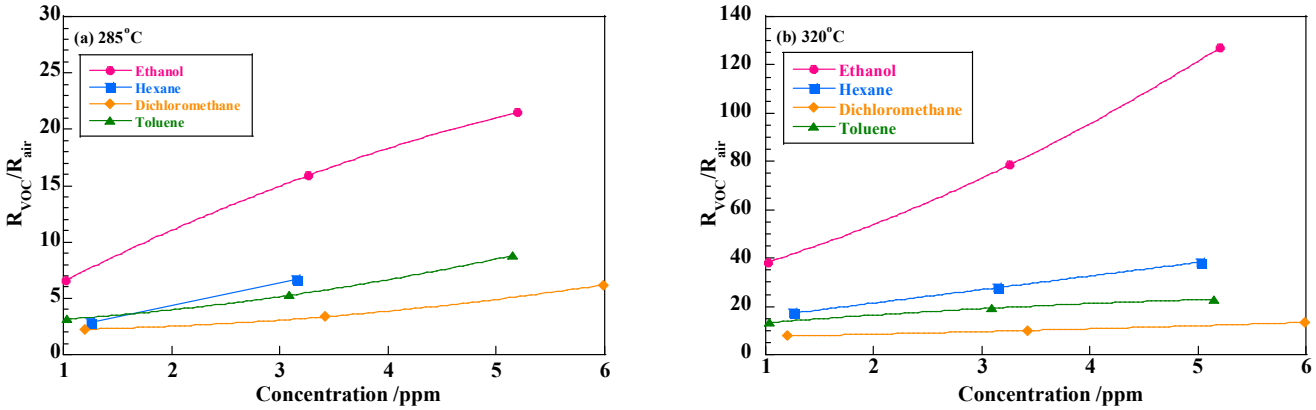

Figure 10. Sensor responses to VOCs with sample B at 285 °C and 320 °C.

3.3. VOC Detection Using p-Type Semiconducting Oxides

VOC detection has been conducted using p-type semiconducting oxides such as NiO [24,25], Co_3O_4 [26] and some perovskite-type oxides [27]. Carbone et al. [24] reported a sensor response of R_{VOC}/R_{air} = 35 at 200 °C to 150 ppm ethanol using NiO grained flowers having a significantly high specific surface area of 240.3 m^2/g. Kruefu et al. [25] obtained the response value of around 40 at 350 °C to 2000 ppm ethanol sensing using Ru-loaded NiO particles with a dimension range of 10–40 nm. Zhang et al. [26] reported the response of 221.99 to 100 ppm ethanol using porous Co_3O_4 with a specific surface area of 28.509 m^2/g. For perovskite-type oxides, $LaFeO_3$ has been tested by some research groups [27,28]. Dai et al. [27] prepared $LaFeO_3$ thin film with the periodic pores of 500 nm in dimension and yielded the response of 14 to 5 ppm ethanol at 450 °C. Yu et al. [28] prepared the Ag-modified $LaFeO_3$ with a specific surface area of 16.45 m^2/g and obtained the response value of 20.9 to 20 ppm ethanol at 180 °C. It is thus obvious that high specific surface area or small particle size of p-type semiconducting oxides is a critical factor for a highly sensitive VOC detection. We previously conducted VOC sensing using the $SmFeO_3$ particle [15]. The $SmFeO_3$ particles possessed the specific surface area of 21.6 m^2/g after the pyrolysis of the cyano-complex at 900 °C in air and the ball-mill crushing process. The sensor response to 3 ppm ethanol was 30 at 400 °C. The $SmFeO_3$ sensor exhibited an outstandingly high response to ethanol of a low concentration. The $SmFeO_3$ powder, in this study, prepared by the ozone-decomposition possesses a comparable surface area without the ball-milling process, that is 17.9 m^2/g. The $SmFeO_3$ sensor based on the ozone-decomposed powder exhibited an even higher response to ethanol, as shown in Figure 10. This suggests that specific surface area is not a sole factor in sensor response. It is predictable that the $SmFeO_3$ particles prepared by the ozone decomposition possess a more favorable surface compared to those by air decomposition.

4. Conclusions

Nano-sized particles of $SmFeO_3$ with larger specific surface area were obtained by pyrolyzing cyano-complex, $Sm[Fe(CN)_6]\cdot 4H_2O$, in ozone at a low temperature of 600 °C. The obtained fine particles possessed a bimodal volume distribution (sample A) and were further classified into finer particles with a unimodal one (sample B). By using the EPD method in the organic suspension with the applied voltage of 3–5 V, $SmFeO_3$ particles were uniformly deposited on the tiny electrode with a dimension of 1.0 × 1.0 mm. The two sensors with samples A and B were tested to detect ethanol and toluene at 285 and 320 °C. The sensors exhibited high responses to ethanol, at around R_{VOC}/R_{air} = 140 at

5 ppm. However, the sensor sample B exhibited a specifically high selectivity to ethanol at 320 °C. We tentatively speculate that the moderately agglomerated morphology of the sample B film selectively reduced the amount of adsorption of toluene. The sensor also exhibited good selectivity of ethanol to hexane and dichloromethane.

Author Contributions: Conceptualization, Y.I. and M.M.; methodology, M.M.; validation, Y.I.; formal analysis, A.N.; investigation, A.N.; resources, Y.I.; data curation, M.M.; writing—original draft preparation, Y.I. and M.M.; writing—review and editing, Y.I.; supervision, Y.I.; project administration, Y.I.; funding acquisition, Y.I. All authors have read and agreed to the published version of the manuscript.

Funding: This research received no external funding.

Institutional Review Board Statement: Not applicable.

Informed Consent Statement: Not applicable.

Data Availability Statement: Not applicable.

Acknowledgments: This work was carried out as a part of the studies in Research Unit for Power Generation and Storage Materials (PGeS) at Ehime University.

Conflicts of Interest: The authors declare no conflict of interest.

References

1. Seiyama, T.; Kato, A.; Fujiishi, K.; Nagatani, M. A New Detector for Gaseous Components Using Semiconductive Thin Films. *Anal. Chem.* **1962**, *34*, 1502–1503. [CrossRef]
2. Yamazoe, N. New approaches for improving semiconductor gas sensors. *Sens. Actuators B Chem.* **1991**, *5*, 7–19. [CrossRef]
3. Matthias, B. Surface science studies of gas sensing materials: SnO_2. *Sensors* **2006**, *6*, 1345–1366.
4. Kim, H.-J.; Lee, J.-H. Highly sensitive and selective gas sensors using p-type oxide semiconductors: Overview. *Sens. Actuators B* **2014**, *192*, 607–627. [CrossRef]
5. Mori, M.; Iwamoto, Y.; Asamoto, M.; Itagaki, Y.; Yahiro, H.; Sadaoka, Y.; Takase, S.; Shimizu, Y.; Yuasa, M.; Shimanoe, K.; et al. Effect of preparation routes on the catalytic activity over $SmFeO_3$ oxide. *Catal. Today* **2008**, *139*, 125–129. [CrossRef]
6. Hui, L.; Futai, M.; Zuzhu, M.; Haiyang, L.; Yabo, X. Study of the reactivity of surface oxygen species on $SmMnO_3$ and $SmFeO_3$ catalysts. *J. Alloys Compd.* **1993**, *193*, 68–69. [CrossRef]
7. Toan, N.; Saukko, S.; Lantto, V. Gas sensing with semiconducting perovskite oxide $LaFeO_3$. *Phys. B Condens. Matter* **2003**, *327*, 279–282. [CrossRef]
8. Aono, H.; Ohmori, J.; Sadaoka, Y. Effects of sintering atmosphere on surface structure and electrical properties of $LaFeO_3$ prepared by thermal decomposition of $La[Fe(CN)_6]\cdot 4H_2O$. *J. Ceram. Soc. Jpn.* **2000**, *108*, 892. [CrossRef]
9. Aono, H.; Traversa, E.; Sakamoto, M.; Sadaoka, Y. Crystallographic characterization and NO_2 gas sensing property of $LaFeO_3$ prepared by thermal decomposition of Ln-Fe hexacyanocomplexes, $Ln[Fe(CN)_6]\cdot 4H_2O$, La, Ln = Nd, Sm, Gd, and Dy. *Sens. Actuators B* **2003**, *94*, 132. [CrossRef]
10. Martinelli, G.; Carotta, M.C.; Ferroni, M.; Sadaoka, Y.; Traversa, E. Screen-printed perovskite-type thick films as gas sensors for environmental monitoring. *Sens. Actuators B Chem.* **1999**, *55*, 99–110. [CrossRef]
11. Traversa, E.; Sadaoka, Y.; Carotta, M.C.; Martinelli, G. Environmental monitoring field tests using screen-printed thick-film sensors based on semiconducting oxides. *Sens. Actuators B Chem.* **2000**, *65*, 181. [CrossRef]
12. Aono, H.; Sato, M.; Traversa, E.; Sakamoto, M.; Sadaoka, Y. Design of Ceramic Materials for Chemical Sensors: Effect of $SmFeO_3$ Processing on Surface and Electrical Properties. *J. Am. Ceram. Soc.* **2004**, *84*, 341–347. [CrossRef]
13. Carotta, M.C.; Martinelli, G.; Sadaoka, Y.; Nunziante, P.; Traversa, E. Gas-sensitive electrical properties of perovskite-type $SmFeO_3$ thick films. *Sens. Actuators B Chem.* **1998**, *48*, 270–276. [CrossRef]
14. Tomoda, M.; Okano, S.; Itagaki, Y.; Aono, H.; Sadaoka, Y. Air quality prediction by using semiconducting gas sensor with newly fabricated $SmFeO_3$ film. *Sens. Actuators B Chem.* **2003**, *97*, 190–197. [CrossRef]
15. Mori, M.; Itagaki, Y.; Iseda, J.; Sadaoka, Y.; Ueda, T.; Mitsuhashi, H.; Nakatani, M. Influence of VOC structures on sensing property of $SmFeO_3$ semiconductive gas sensor. *Sens. Actuators B Chem.* **2014**, *202*, 873–877. [CrossRef]
16. Hosoya, Y.; Itagaki, Y.; Aono, H.; Sadaoka, Y. Ozone detection in air using $SmFeO_3$ gas sensor. *Sens. Actuators B Chem.* **2005**, *108*, 198–201. [CrossRef]
17. Mathe, V.L. Structural, dielectric and electrical properties of $Sm_xBi_{1-x}FeO_3$ ceramics. *J. Magn. Magn. Mater.* **2003**, *263*, 344–352. [CrossRef]
18. Ishihara, T.; Sato, K.; Takita, Y. Electrophoretic Deposition of Y_2O_3-Stabilized ZrO_2 Electrolyte Films in Solid Oxide Fuel Cells. *J. Am. Ceram. Soc.* **1996**, *79*, 913–919. [CrossRef]

19. Sing, K.S.W.; Everett, D.H.; Haul, R.A.W.; Moscou, L.; Pierotti, R.A.; Rouquerol, J.; Siemieniewska, T. Reporting physisorption data for gas/solid systems with special reference to the determination of surface area and porosity (Recommendations 1984). *Pure Appl. Chem.* **1985**, *57*, 603–619. [CrossRef]
20. Gregg, S.J.; Sing, K.S.W.; Salzberg, H.W. *Adsorption, Surface Area and Porosity*, 2nd ed.; Academic Press: London, UK, 1982.
21. Li, H.; Yu, K.; Lei, X.; Guo, B.; Li, C.; Fu, H.; Zhu, Z. Synthesis of the MoS_2@CuO heterogeneous structure with improved photocatalysis performance and H_2O adsorption analysis. *Dalton Trans.* **2015**, *44*, 10438–10447. [CrossRef]
22. Yamazoe, N.; Shimanoe, K. Theory of power laws for semiconductor gas sensors. *Sens. Actuators B Chem.* **2008**, *128*, 566–573. [CrossRef]
23. Itagaki, Y.; Fujihashi, K.; Aono, H.; Mori, M.; Sadaoka, Y. VOC sensing behavior of semiconducting Sm_2O_3/$SmFeO_3$ mixtures. *J. Ceram. Soc. Jpn.* **2015**, *123*, 961–966. [CrossRef]
24. Carbone, M.; Tagliatesta, P. NiO Grained-Flowers and Nanoparticles for Ethanol Sensing. *Materials* **2020**, *13*, 1880. [CrossRef]
25. Kruefu, V.; Wisitsoraat, A.; Phokharatkul, D.; Tuantranont, A.; Phanichphant, S. Enhancement of p-type gas-sensing performance of NiO nanoparticles prepared by precipitation with RiO_2 impregnation. *Sens. Actuators B Chem.* **2016**, *236*, 466–473. [CrossRef]
26. Zhang, X.; Xu, Y.; Liu, H.; Zhao, W.; Ming, A.; Wei, F. Preparation of porous Co_3O_4 and its response to ethanol with low energy consumption. *RSC Adv.* **2020**, *10*, 2191–2197. [CrossRef]
27. Dai, Z.; Lee, C.-S.; Kim, B.-Y.; Kwak, C.-H.; Yoon, J.-W.; Jeong, H.-M.; Lee, J.-H. Honeycomb-like Periodic Porous $LaFeO_3$ Thin Film Chemiresistors with Enhanced Gas-Sensing Performances. *ACS Appl. Mater. Interfaces* **2014**, *6*, 16217–16226. [CrossRef]
28. Yu, J.; Wang, C.; Yuan, Q.; Yu, X.; Wang, D.; Chen, Y. Ag-Modified Porous Perovskite-Type $LaFeO_3$ for Efficient Ethanol Detection. *Nanomaterials* **2020**, *12*, 1768. [CrossRef] [PubMed]